

Driver-centric Risk Object Identification

Chengxi Li, *Member, IEEE*, Stanley H. Chan, *Senior Member, IEEE*, and Yi-Ting Chen, *Member, IEEE*

Abstract—A massive number of traffic fatalities are due to driver errors. To reduce fatalities, developing intelligent driving systems assisting drivers to identify potential risks is in urgent need. Risky situations are generally defined based on collision prediction in existing research. However, collisions are only one type of risk in traffic scenarios. We believe a more generic definition is required. In this work, we propose a novel driver-centric definition of risk, i.e., risky objects influence driver behavior. Based on this definition, a new task called risk object identification is introduced. We formulate the task as a cause-effect problem and present a novel two-stage risk object identification framework, taking inspiration from models of situation awareness and causal inference. A driver-centric Risk Object Identification (ROI) dataset is curated to evaluate the proposed system. We demonstrate state-of-the-art risk object identification performance compared with strong baselines on the ROI dataset. In addition, we conduct extensive ablative studies to justify our design choices.

Index Terms—Risk assessment, driving scene understanding, situation awareness, end-to-end driving model, and causal inference

1 INTRODUCTION

More than 1.3 million people die in road accidents worldwide every year, or approximately 3,700 people per day [1]. Road traffic accidents are among the leading causes of non-natural death around the world. The majority of these accidents are due to driver errors, such as lack of awareness [2]. To reduce the number of accidents, developing intelligent driving systems that identify potential hazards is in urgent need. The task has been studied extensively in the risk assessment literature [3]. In the context of intelligent vehicles, the risk is generally defined based on collision prediction. While this definition is widely applied, road collision is only one source of potential hazards in driving [3]. We believe a more generic definition is needed.

We propose a novel driver-centric definition of risk, i.e., *risky objects influence driver behavior*. Fig. 1 depicts the idea of the proposed definition. While driving toward an intersection, we react to the crossing pedestrian (i.e., slow down). After passing the intersection, we react to the construction cone (i.e., deviate to a clear path). From these examples, we observe that we constantly attend to those traffic participants potentially influencing driver behavior, because we humans are equipped with risk perception. In other words, a dangerous situation would occur if we do not react to them immediately. The proposed definition captures the observation. We believe the definition gives a new perspective to the definition of risk assessment.

A natural question arises: *Who changes drivers' behavior?* We propose a new task called *risk object identification*, which aims to identify the object(s) influencing drivers' behavior. The proposed task can be approached via three existing tasks: (1) salient object identification learned from human

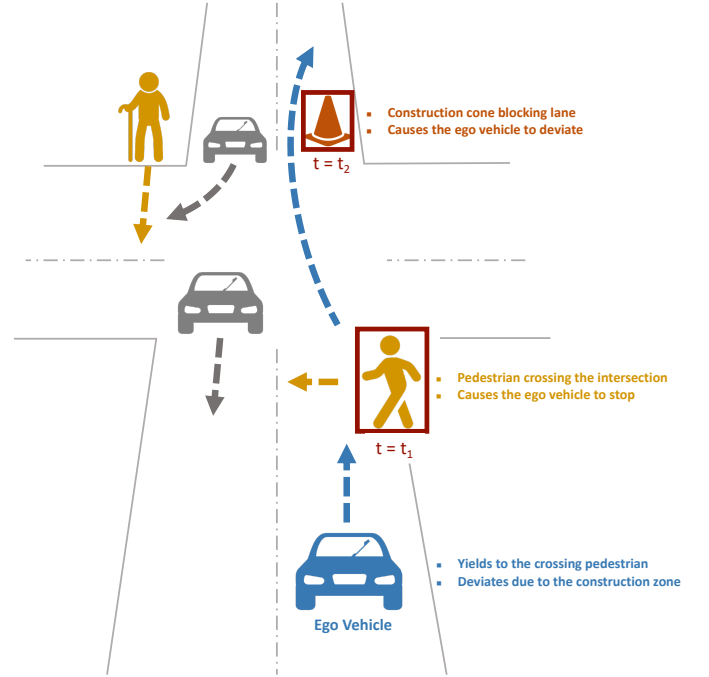


Fig. 1. Human drivers perceive scenes, assess risks, make a plan, and take actions while driving. Risk assessment, identifying hazards and risk factors that have the potential to cause harm, is indispensable for driving safety. In this work, we cast the identification of potential hazards as a cause-effect problem. A new task called risk object identification is introduced. We propose a novel computational framework that learns to reason how humans react (effect) to these objects (cause).

gaze behavior [4]; (2) object importance estimation or risky region localization learned from human annotations [5], [6]; and (3) salient regions/objects identification learned from end-to-end driving models with self-attention mechanisms [7], [8].

First, learning to predict pixel-level driver attention by imitating human gaze behavior has been explored by [4], [9], [10]. This area of research is motivated by psychological studies suggesting that there is a connection between driving, attention, and gaze [11]. Alletto et al., [4] collect a

- C. Li and S. H. Chan are with the Department of Electrical and Computer Engineering, Purdue University, West Lafayette, IN, 47906. Email: li2509, stanchan@purdue.edu
- Y.-T. Chen is with National Yang Ming Chiao Tung University and National Chiao Tung University, Hsinchu, Taiwan. Email: ychen@nycu.edu.tw.
- A part of the work was done when C. Li was an intern and Y.-T. Chen was a research scientist at Honda Research Institute USA, San Jose, CA, USA.

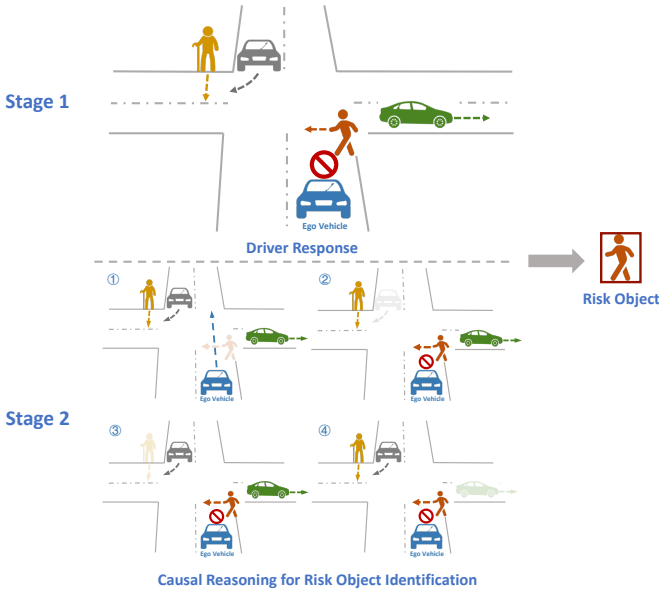


Fig. 2. An conceptual diagram of the proposed two-stage risk object identification framework. We first predict driver response in a given situation. To identify object(s) influencing driver behavior, we intervene the input observation by removing a traffic participant at a time (i.e., simulating a situation with the traffic participant), and predict the corresponding driver response. For instance, removing the crossing pedestrian changes driver response (effect) from *Influenced* to *Uninfluenced*. The effects of removing other traffic participants remain the same. We conclude that the crossing pedestrian is the risk object (cause).

large-scale dataset including drivers’ gaze fixations acquired during actual driving. While the direction of this study is promising, human gaze behavior is intrinsically noisy, and fixations may not directly associate with objects influencing drivers’ behavior. Second, risky region localization [6] or object importance estimation [5] formulate the task as a two-class object detection problem. Human annotators are asked to label risky regions or important objects. While favorable results are obtained, the supervised learning-based formulation requires a significant amount of human-labeled annotations, and the performance in unseen situations cannot be guaranteed. Third, the task can be formulated as selecting regions/objects with high activations in visual attention heat maps learned from end-to-end driving models [7], [8]. human periphery and fovea visual system, Xia et al. [9] propose . Specifically, pixel- and object-level attention maps are obtained via optimizing task-driven objective functions and self-attention mechanisms. However, highly activated objects/regions do not necessarily associate with models’ decisions. The issue outlines the confusion between causation and correlation. In [12], the authors also identify “causal misidentification” as an under-explored problem in training end-to-end driving models.

To address the aforementioned issues, we propose a novel two-stage risk object identification framework based on the proposed definition of risk. Specifically, we formulate the risk object identification as a cause-effect problem [13]. The core concept is depicted in Fig. 2. In the first stage, a driving model learns to predict driver response in a given situation. We simplify the response of drivers to be *Influenced* or *Uninfluenced*. In this paper, we denote *Influenced*

or *Uninfluenced* as *Stop* and *Go*, respectively. To predict driver response, a novel driving model motivated by the model of situation awareness [14] is proposed. Specifically, the proposed model encapsulates the goal (i.e., driver intention), perception (i.e., elements of the environment), comprehension (i.e., interactions between driver and *Thing* objects and interactions between driver and *Stuff* objects in 3D), and projection (i.e., intention-aware interaction forecasting) for driver response prediction. *Thing* and *Stuff* objects are defined in Section 5.1.

In the second stage, given a *Stop* response (i.e., driver behavior is influenced by certain objects), we intervene input video by removing a tracklet at a time and inpainting the removed area in each frame to simulate a scenario without the presence of the tracklet. The same driving model is applied to predict the effect of the removal. The process iterates through all tracklets and records the corresponding effects. Please note that we assume that the cause of driver response change is either vehicles or pedestrians. The tracklet that causes a maximum response change is the risk object.

Our work differs from existing methods [4], [5], [6], [7], [8] in the following three aspects:

- 1) A novel driver-centric notion of risk, whereby risky objects are defined as those that influence driver behavior, is proposed;
- 2) An unsupervised framework is introduced as an initial step toward generalization;
- 3) A causal inference-based framework is proposed to address the issue of “causal misidentification” in end-to-end driving models for risk object identification.

In this work, we make the following substantial extensions to our early results [15]:

- 1) We re-design the driving model substantially to predict driver response by modeling driver decision processes via the model of situation awareness [14];
- 2) We systematically benchmark three different tasks, i.e., driver response prediction, driver intention prediction, and risk object identification on the proposed driver-centric ROI dataset;
- 3) We conduct thorough ablative studies to justify the architectural designs.

2 RELATED WORK

Risk Assessment. Living agents can assess risk for decision-making. Earlier attempts have been made to study this problem from different angles, and can be categorized into four categories. First, the works [16], [17] design a set of rules based on the current state of vehicles and contextual states for detecting dangerous situations. These rule-based approaches ignore uncertainties of dynamic driving environments, leading to instabilities in their decisions. Second, risky situations can be determined by the similarity of a pattern between a pair of traffic participants with accident patterns obtained from accident databases [18], [19]. However, real-world accident data are hard to obtain. It is also challenging to realistically simulate accident with a simulator. Moreover, it is insufficient to consider pairwise relations in complicated driving scenarios, where multiple traffic participants interact with each other.

Third, a popular risk assessment methodology is to predict all possible colliding future trajectories [20], [21], [22]. Please refer to [3] for a detailed survey of motion prediction and risk assessment in the context of intelligent vehicles. While predicting all possible colliding future trajectories is well-received by this research field, the approach involves a large number of computations since it requires pairwise comparisons. Fourth, Lefèvre et al. [23] define the risk of a situation by detecting conflicts between driver intention and expectation via a probabilistic framework. While this paradigm is very close to our proposed definition of risk, the underlying mechanism for risk object identification is different. Specifically, in [23], a risk object is identified by computing the probability of intention-expectation mismatch for each vehicle based on vehicle states. If the probability exceeds a threshold, the corresponding vehicle is considered to be a “hazard”. In contrast, we discover the risk object based on causal inference, reasoning the effect of an object removal (i.e., intervention).

Vision-based End-to-end Driving Models. The history of vision-based end-to-end driving models can be traced back to 1989 when ALVINN [24], the framework that learns a mapping from images to navigation signals via a shallow neural network, is introduced. Recently, Bojarski et al. [25] demonstrate a similar idea by extending it to modern convolutional neural networks for extracting better visual representations from images. In [26], visual representations are learned with an auxiliary semantic segmentation task to better represent driving scenes.

While significant progress has been demonstrated, neural network-based frameworks lack interpretability, crucial for safety-critical applications. To address the issue, Kim et al. [7], [27] and Wang et al., [8] propose pixel- and object-level attention mechanisms, respectively. Particularly, Wang et al., [8] propose an object-level attention scoring mechanism as a means to model how certain traffic participants impact actions of driving models.

Interactions modeling between traffic participants is commonly studied in trajectory prediction literature [28], [29], [30], [31]. However, interaction modeling for learning driving policies is under-explored. To address this problem, our method explicitly models the interactions using Graph Convolutional Networks (GCNs). Instead of simply weighting and concatenating objects’ visual representations as interaction modeling [8], we model interaction as message passing that incorporates relative distances between traffic participants and ego-vehicle. Moreover, interactions between the ego-vehicle and road infrastructure (e.g., traffic light) are considered in the proposed framework. We show that the two interaction modelings are essential for driver response prediction. Additionally, the proposed driving model exploits the inductive biases motivated by situation awareness [14]. We empirically demonstrate the effectiveness of these inductive biases for both driver response prediction and risk object identification.

While the aforementioned driving models have shown remarkable advances in following roads and avoiding obstacles, they cannot be guaranteed to achieve a goal (e.g., left turn). Codevilla et al. [32], [33] incorporate navigational commands as an extra input for learning driving policies.

Instead of inputting a navigational command, the proposed driving model infers drivers’ intention from egocentric videos for driver response prediction.

Causality in Computer Vision. Computer vision research has proliferated over the past decades due to the advance of deep learning algorithms. However, current deep learning models suffer from spurious correlation problems [34] because of ignoring causality in data. Humans perceive causality of the physical world. To address the issue, recent studies [35], [36], [37], [38], [39] explicitly consider the concept of causality into deep learning architectural designs.

Particularly, the authors of [37], [38] propose a novel training objective as a practical approximation for imaginative intervention (i.e., *do* operator proposed in [13]) to eliminate noncausal relations and unobserved confounders for image captioning and visual Q&A. In this work, we also leverage causal intervention but in a different way. Specifically, instead of using an imaginative causal intervention, we explicitly conduct *do* operator via image inpainting.

To our best knowledge, we are among the first to utilize causal inference for driving scene applications. Kim et al. [7] propose a causality test to verify the effectiveness of inferred attention maps obtained from the proposed driving model. We also employ causal inference similar to the causality test. However, the purpose of causal inference in this work is to identify risk objects. Moreover, we design a simple but effective data augmentation strategy using causal intervention. This leads to a more robust driving model.

Haan et al. [12] propose to incorporate functional causal models [13] into imitation learning to address the issue of “causal misidentification”. In [40], they overcome the causal misidentification issue by adding noises to inputs. Our work is complementary to [12], [40]. Specifically, the focus of [12], [40] is to improve the robustness of driving models, whereas the proposed framework leverages driving models to determine the response of drivers in a counterfactual situation for risk object identification. We believe the two lines of work should be studied jointly and will leave for future work.

3 DRIVER-CENTRIC ROI DATASET

To study driver-centric risk object identification, a dataset with diverse reactive scenarios (i.e., drivers react to potential hazards while navigating to their goals) is indispensable. For instance, when human drivers intend to turn left at an unprotected intersection, we react (e.g., slowing down or stopping) to certain traffic participants to avoid dangerous situations. We curate a driver-centric Risk Object Identification (ROI) dataset from the Honda Research Institute Driving Dataset (HDD) [41]¹.

3.1 Dataset Annotation

The driver-centric ROI dataset utilizes a two-layer representation — **Intention** and **Response**. Fig. 3 illustrates how we construct the proposed driver-centric ROI dataset from the HDD dataset.

The **Goal-oriented** layer defined in the HDD dataset denotes tactical driver behavior such as *right turn*, *left turn*,

1. The dataset is available at <https://usa.honda-ri.com/HDD>

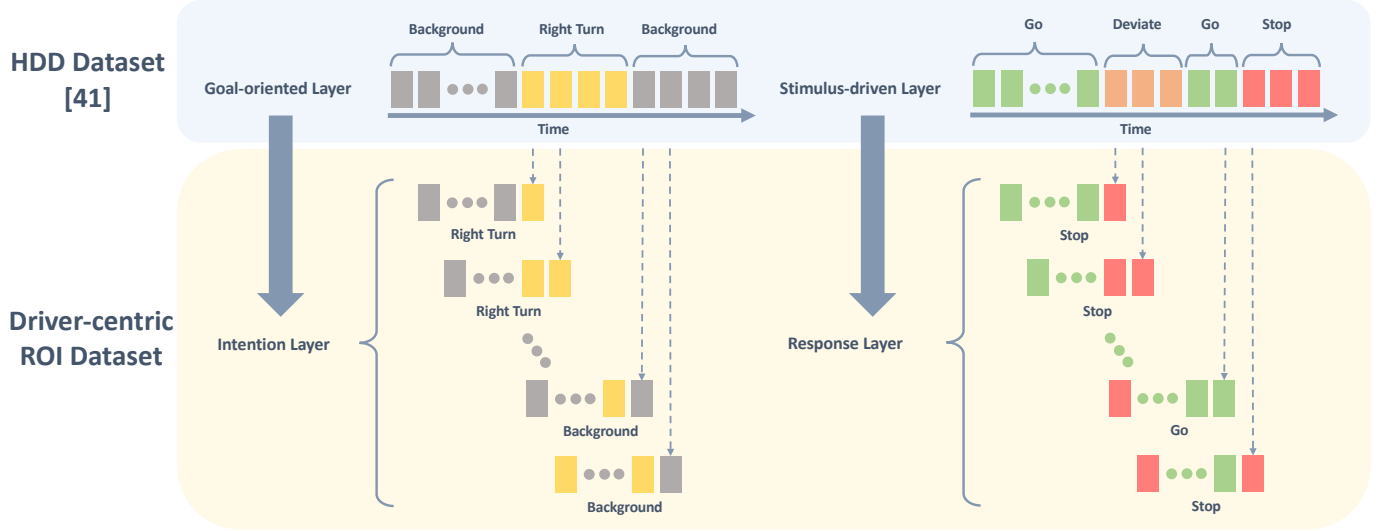


Fig. 3. Driver-centric Risk Object Identification (ROI) dataset. To study risk object identification, a dataset with a diverse of reactive scenarios is essential. We build the driver-centric ROI dataset on top of the Honda Research Institute Driving Dataset (HDD). In particular, we introduce two layers, i.e., **Driver Intention** and **Driver Response** in the proposed dataset. Further detail of the two layers can be found in Section 3. To obtain **Intention** labels, we form n -frame clips, and the corresponding **Intention** label of each clip is the last frame’s label defined in the **Goal-oriented** layer. A similar procedure is applied to construct the **Response** layer (as shown on the right-hand side of the figure). Notice that both *Stop* and *Deviate* annotated in HDD are merged into *Stop* in our dataset.

Split	Intention												Response	
	BG	IP	LT	RT	LLC	RLC	LLB	RLB	CP	RP	MG	UT	STP	G
Train	737 949	48 933	21 819	19 824	4 815	4 386	1 833	717	2 364	588	1 182	2 001	184 890	661 521
Test1	236 622	17 772	7 017	6 195	1 098	1 212	435	324	432	123	327	432	63 314	208 675
Test2	Cause													
	Congestion	98	/	/	/	1	/	/	/	/	/	/	99	/
	Crossing Pedestrian	62	15	5	/	/	/	/	2	/	/	/	84	/
	Crossing Vehicle	263	2	7	35	/	/	4	/	/	/	/	311	/
	Parked Vehicle	120	3	/	/	9	4	/	/	/	/	/	136	/
All		543	20	12	35	10	4	/	4	2	/	/	630	/
Intention: (BG) background, (IP) intersection passing, (LT) left turn, (RT) right turn,(LLC) left lane change, (RLC) right lane change, (LLB) left lane branch, (RLB) right lane branch,(CP) crosswalk passing, (RP) railroad passing, (MG) merge, (UT) u-turn. Response: (STP) stop, (G) go.														

TABLE 1
Statistics (annotated frames) of the proposed driver-centric ROI dataset.

or *lane change*. As shown in Fig. 3, each frame is labeled with either a goal-oriented or background action. To obtain the **Intention** of a n -frame clip (the parameter n is 20 in our implementation), we use the last frame’s label of the **Goal-oriented** layer as the **Intention** label. While performing a tactical behavior, drivers might have to *stop* or *deviate* due to traffic participants or obstacles. We extend the **Stimulus-driven** actions, i.e., *Stop* and *Deviate*, defined in the HDD dataset as the **Response** label. Note that both *Stop* and *Deviate* are merged into *Stop* as depicted in Fig. 3. The rest of the frames are labeled as *Go*. The HDD dataset also annotates a **Cause** layer to explain the reason for *Stop* and *Deviate* actions. We create our **Test2** set by selecting frames from the four **Cause** scenarios, i.e., *Congestion*, *Crossing Pedestrian*, *Crossing Vehicle* and *Parked Vehicle*. Moreover, in the **Test2** set, we provide bounding boxes of risk objects (i.e., object[s] influencing driver’s behavior) for risk object identification

benchmarks. We focus on scenarios in which drivers react to vehicles or pedestrians.

3.2 Dataset Statistics

The driver-centric ROI dataset has 184 890 frames for training driver response and intention predictors. Two test sets are constructed for driver response prediction and risk object identification, respectively. The **Test1** split has 63,314 frames for both driver response and intention benchmarks. The **Test2** has 630 frames (i.e., 630 different risk objects) covering four different reactive scenarios, i.e., *Congestion*, *Crossing Pedestrian*, *Crossing Vehicle*, and *Parked Vehicle* for risk object identification benchmarks. Detailed statistics are shown in Table 1.

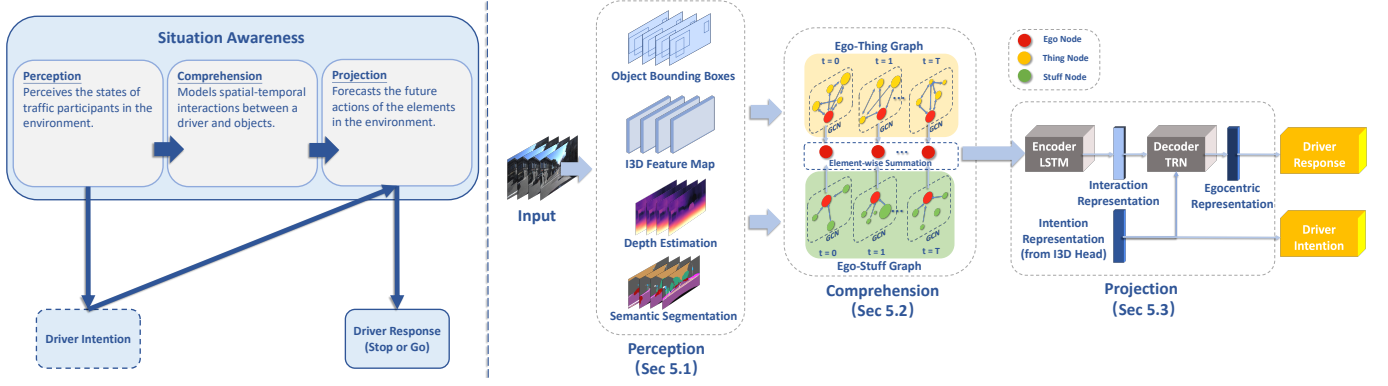


Fig. 4. An overview of the proposed intention-aware driving model for driver response prediction (right). The proposed architecture is motivated by the model of situation awareness [14] (left). Given a video clip, 3D convolutions (I3D), object detection, semantic segmentation, and depth estimation are applied to obtain states of traffic participants in a traffic environment at the *Perception* stage (Sec. 5.1). At the *Comprehension* stage, an *Ego-Thing Graph* and an *Ego-Stuff Graph* are constructed to model spatial-temporal interactions between a driver and traffic participants (Sec. 5.2). In this work, we categorize traffic participants into two types, i.e., *Thing* and *Stuff*. The details are discussed in Sec. 5.2. The final stage, *Projection* (Sec. 5.3), forecast future interactions between driver and traffic participants for driver response prediction. Frame-wise interactions obtained from *Ego-Thing Graph* and *Ego-Stuff Graph* are fused and fed into an encoder LSTM to form interaction representation. Intention representation obtained from the I3D head and interaction representation are sent a decoder TRN (the architecture is shown in Fig. 5) to predict driver response.

4 PROBLEM FORMULATION

Given a reactive scenario with T RGB images $I := \{I_1, I_2, \dots, I_T\}$, the goal is to identify the object influencing driver response in the last frame. The task is called risk object identification.

We formulate the task as a cause-effect problem [13]. Specifically, a two-stage framework is proposed to identify the cause (i.e., the object) of an effect (i.e., driver response) via the proposed *Intention-aware Driving Model* and *Causal Reasoning for Risk Object Identification*. We discuss the methodology in the following.

5 INTENTION-AWARE DRIVING MODEL

An overview of the proposed intention-aware driving model is depicted in Fig. 4. To predict the response of a driver, a driving model should capture complicated spatio-temporal interactions between a driver and traffic participants. We propose a novel driving model motivated by the model of situation awareness (SA) [14]. Specifically, the proposed model encapsulates the four essential components defined in SA for driver response prediction: goal/objective (i.e., driver intention), perception (i.e., elements of a traffic environment), comprehension (i.e., interactions between driver and *Thing* objects, and interactions between driver and *Stuff* objects in 3D), and projection (i.e., intention-aware interaction forecasting). The detail of each component is discussed in the following.

5.1 Perception

Perception plays an essential role in the SA model [14]. This component perceives the status, attributes, and dynamics of relevant traffic participants of a traffic environment. Specifically, given T RGB images, we apply object detection [42] and semantic segmentation [43] to obtain *Thing* and *Stuff* objects, respectively. In this work, we distinguish *Stuff* objects from *Thing* objects by evaluating whether states of an object can be influenced by other objects. If yes, we

categorize the object as a *Thing* object. For instance, cars stop or yield to pedestrians, but a traffic light turns red or green by itself. In addition to detection and segmentation, we perform object tracking using Deep SORT [44] and depth estimation [45].

5.2 Comprehension

We interpret *Comprehension* as the spatio-temporal interactions between the driver and *Thing* objects, and interactions between the driver and *Stuff* objects in the 3D world. Note that a thorough modeling of *Comprehension* is beyond the scope of this work. Specifically, we construct two graphs, i.e., *Ego-Thing Graphs* and *Ego-Stuff Graphs*. They are modeled with Graph Convolutional Networks (GCNs) [46]. The details of each graph are discussed below. Note that the interaction modeling is proposed in [47]. We extend the modeling for driver response prediction.

5.2.1 Ego-Thing Graph

The *Ego-Thing Graph* is designed to model interactions among a driver and *Thing* objects.

Graph Definition. We denote a sequence of frame-wise *Ego-Thing Graphs* as $\mathbf{G}^{ET} = \{\mathbf{G}_t^{ET} | t = 1, \dots, T\}$, where T is the number of frames, and $\mathbf{G}_t^{ET} \in \mathbb{R}^{(K+1) \times (K+1)}$ is the *Ego-Thing* affinity matrix at frame t encoding pair-wise interactions among *Thing* objects and *Ego*. Specifically, $G_t^{ET}(i, j)$ denotes the influence of object j on object i . A Node i at time t is represented by two types of features $(\mathbf{x}_i^t, \mathbf{p}_i^t)$, where \mathbf{x}_i^t represents the appearance feature, and $\mathbf{p}_i^t \in \mathbb{R}^{1 \times 3}$ is the 3D location of the i -th object in respect to *Ego* in a local frame.

Node Feature Extraction. *Thing* objects are *car*, *person*, *bicycle*, *motorcycle*, *bus*, *train*, and *truck*. Given bounding boxes obtained from object detection [42], we keep K top-scoring detected boxes. The parameter K is set to 20. There are $K + 1$ objects, where index $i = 1, 2, \dots, K$ corresponds to *Thing* objects, and index $K + 1$ corresponds to

Ego. The appearance feature for i -th object is denoted as $\mathbf{x}_i^t \in \mathbb{R}^{1 \times D}$, $i = 1, 2, \dots, K, K+1$. RoAlign [42] and max pooling are applied to obtain the appearance features of *Thing* objects. The appearance of *Ego* is obtained by the same procedure as *Thing* objects, but with a frame-size bounding box.

Relational Modeling. We consider both appearance features and distance constraints motivated by [48] in relational modeling. An edge $G_t^{ET}(i, j)$ is defined as:

$$G_t^{ET}(i, j) = \frac{f_s(\mathbf{p}_i^t, \mathbf{p}_j^t) \exp(f_a(\mathbf{x}_i^t, \mathbf{x}_j^t))}{\sum_{j=1}^{K+1} f_s(\mathbf{p}_i^t, \mathbf{p}_j^t) \exp(f_a(\mathbf{x}_i^t, \mathbf{x}_j^t))}, \quad (1)$$

where $f_a(\mathbf{x}_i^t, \mathbf{x}_j^t)$ indicates an appearance relation, and $f_s(\mathbf{p}_i^t, \mathbf{p}_j^t)$ denotes relative distance between i -th and j -th object, respectively. The softmax function is used to normalize an affinity matrix G_t^{ET} . An appearance relation is defined as below:

$$f_a(\mathbf{x}_i^t, \mathbf{x}_j^t) = \frac{\phi(\mathbf{x}_i^t)^T \phi'(\mathbf{x}_j^t)}{\sqrt{D}}, \quad (2)$$

where $\phi(\mathbf{x}_i^t) = \mathbf{w}\mathbf{x}_i^t$ and $\phi'(\mathbf{x}_j^t) = \mathbf{w}'\mathbf{x}_j^t$. Both $\mathbf{w} \in \mathbb{R}^{D \times D}$ and $\mathbf{w}' \in \mathbb{R}^{D \times D}$ are learnable parameters. \sqrt{D} is a normalization factor.

In addition to appearance relation, we also consider spatial constraint via calculating a relative distance between a pair of objects. Specifically, we unproject the center of a *Thing* object's bounding box to 3D space [45]. For *Ego*, we unproject the middle-bottom pixel of the frame to 3D space. Given a 2D coordinate (u_i^t, v_i^t) of i -th object at time t , the corresponding 3D coordinate (x_i^t, y_i^t, z_i^t) is obtained as follows:

$$\begin{bmatrix} x_i^t & y_i^t & z_i^t & 1 \end{bmatrix}^T = \delta_{u_i^t, v_i^t} \cdot \mathbf{P}^{-1} \begin{bmatrix} u_i^t & v_i^t & 1 \end{bmatrix}^T, \quad (3)$$

where \mathbf{P} is the camera intrinsic matrix, and $\delta_{u_i^t, v_i^t}$ is the relative depth at (u_i^t, v_i^t) obtained by [45]. The spatial constraint f_s is formulated as:

$$f_s(\mathbf{p}_i^t, \mathbf{p}_j^t) = \mathbb{I}(d(\mathbf{p}_i^t, \mathbf{p}_j^t) \leq \mu), \quad (4)$$

where \mathbf{p}_i^t denotes the 3D coordinate of i -th object at time t , $\mathbb{I}(\cdot)$ is the indicator function, $d(\mathbf{p}_i^t, \mathbf{p}_j^t)$ computes the Euclidean distance between object i and object j in the 3D space, and μ is the distance threshold. The motivation of spatial constraint is that interactions between two distant objects are usually scarce. In our implementation, we empirically set the value of μ to be 3.0.

5.2.2 Ego-Stuff Graph

An *Ego-Stuff Graph* \mathbf{G}^{ES} is constructed in a similar manner as an *Ego-Thing Graph* \mathbf{G}^{ET} except for node feature extraction.

Node feature extraction. We define the following classes as *Stuff* objects: *Crosswalk*; *Lane Markings*; *Lane Separator*; *Road*; *Service Lane*; *Traffic Island*; *Traffic Light* and *Traffic Sign*. Some *Stuff* classes (e.g., crosswalk obtained from semantic segmentation) cannot be well depicted as rectangular bounding boxes. Thus, RoAlign [42] is not applicable. We propose MaskAlign to extract features from a binary mask \mathbf{M}_i^t , i.e., the i -th *Stuff* object at time t . MaskAlign first downsamples

the mask \mathbf{M}_i^t to the same spatial dimension of an intermediate 3D feature map \mathbf{X} . Note that the downsampled mask is denoted as $\mathbf{M}_i^{t'}$. A *Stuff* object feature is obtained as follows:

$$\mathbf{x}_i^t = \frac{\sum_{w=1}^W \sum_{h=1}^H \mathbf{X}_{(w,h)}^t \cdot \mathbf{M}_i^{t'}(w,h)}{\sum_{w=1}^W \sum_{h=1}^H \mathbf{M}_i^{t'}(w,h)}, \quad (5)$$

where $\mathbf{X}_{(w,h)}^t \in \mathbb{R}^{1 \times D}$ is a D -dimension feature at location (w, h) for time t , and $\mathbf{M}_i^{t'}(w, h)$ is a binary scalar indicating whether object i exists at location (w, h) .

Relational Modeling. We neglect interactions among *Stuff* objects since they are insusceptible to each other. We only model interactions between *Stuff* objects and *Ego*. Hence, we set f_s (as in Eq. 4) to zeros for every pair of *Stuff* objects. To model spatial constraint, we unproject every pixel within a downsampled binary mask $\mathbf{M}_i^{t'}$ to the 3D space, and calculate the relative distance between the corresponding 3D coordinates and the 3D coordinate of *Ego*. We choose the one with the minimum distance within a downsampled mask. The distance threshold μ in *Ego-Stuff Graphs* is empirically set to be 0.6.

5.2.3 Interaction Modeling as Message Passing

In Section 5.2.1 and 5.2.2, two relational modelings are discussed. To predict driver response, we need interaction modeling that captures influences of multiple traffic participants to a driver. We formulate interactions as message passing in GCN that takes a graph as input, passes information through edges, and outputs updated nodes' features. The message passing process in GCN is written as:

$$\mathbf{X}^{l+1} = \mathbf{G}\mathbf{X}^l\mathbf{W}^l + \mathbf{X}^l, \quad (6)$$

where \mathbf{G} is the affinity matrix discussed in Section 5.2.1 and 5.2.2. The matrix $\mathbf{X}^l \in \mathbb{R}^{(K+1) \times D}$ is the appearance feature matrix for the l -th layer. $\mathbf{W}^l \in \mathbb{R}^{D \times D}$ is a learnable weight matrix. We also build a residual connection by adding \mathbf{X}^l . Layer Normalization [49] and ReLU are applied before \mathbf{X}^{l+1} is fed to the next message passing. Note that we use a one-layer GCN to model *Ego-Stuff* interactions and a two-layer GCN for *Ego-Thing* interaction modeling.

5.3 Projection

The role of *Projection* is to forecast future actions of elements in the environment. The updated appearance feature \mathbf{X}^{l+1} , discussed in the *Comprehension* section, is processed independently at every frame without considering temporal changes. An encoder-decoder architecture is proposed to capture temporal interactions for forecasting future interactions.

Encoder-decoder Architecture. We implement the proposed encoder-decoder architecture based on the Temporal Recurrent Network (TRN) [50], which makes use of both accumulated historical evidence and predicted future information to better predict current action. Following [50], we use long short-term memory (LSTM) [51] as the backbone for both encoder and decoder.

We aggregate updated *Ego* features from *Ego-Stuff Graphs* and *Ego-Thing Graphs* by an element-wise summation. Time-specific updated *Ego* features are fed into the encoder LSTM

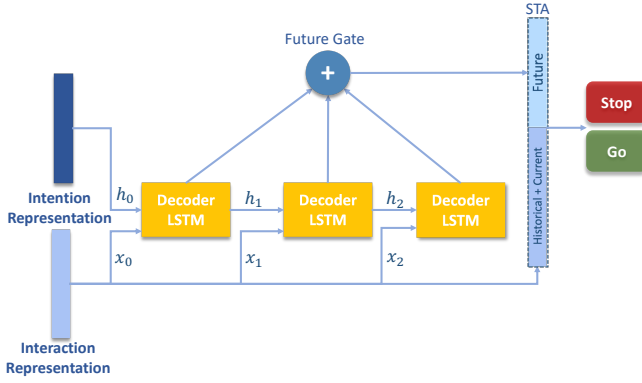


Fig. 5. Decoder Temporal Recurrent Network (TRN) [50]. The inputs to this module are intention and interaction representations. Note that intention representation is used to initialize the hidden state of the first decoder LSTM cell. The future gate and spatiotemporal accumulator (STA) aggregate features from historical, current, and predicted future information to predict driver response.

to obtain a $1 \times D$ feature vector called interaction representation. Note that prior works [48], [52], [53] fuse all nodes' features in a graph, and the fused features are sent to the encoder LSTM. In contrast, we only send updated *Ego* features in \mathbf{X}^{l+1} to the encoder-decoder architecture, because updated *Ego* features are expected to capture interactions among traffic participants that are key to robust driver response prediction. Unlike typical decoder architectures implemented as other LSTMs, TRN includes an LSTM decoder, a future gate, and a spatiotemporal accumulator (STA). We extend TRN for the predicting driver response, and the corresponding architecture is depicted in Fig. 5. The LSTM decoder learns a feature representation of the evolving interactions. The future gate receives a vector of hidden states from the decoder LSTM and embeds features via the element-wise summation as the future context. The STA concatenates historical, current, and predicted future spatiotemporal features, and estimates driver response occurring in the very next frame.

Intention-aware Design. Driver intention is indispensable for planning the next action [32], estimating the importance of road users [54], and assessing risk [55]. Similarly, in our task, driver response (i.e., *Go* and *Stop*) is determined not only by interactions among traffic participants but also driver intention (e.g., *Left Turn* or *Right Turn*). For instance, a vehicle turning right at an intersection will not stop for pedestrians walking on the left sidewalk. Hence, we treat features extracted from the I3D head as the intention representation. The representation is used to initialize the hidden state of the first decoder LSTM cell. Note that the design differs from [50], which initializes the hidden state h_0 with zeros. To acquire a good intention representation, the representation is trained to predict driver intention in a supervised learning manner.

6 CAUSAL REASONING

The previous section introduces the proposed intention-aware driving model. In this section, we discuss how we utilize *intervention*, a powerful tool for causal inference, as

Algorithm 1 Driving Model Training

T : Number of frames
 N : Number of *Thing* objects in a given tracklet list
 \mathbf{A}_r : Ground truth driver response (either *Go* or *Stop*)
Input: A sequence of RGB frames $I := \{I_1, I_2, \dots, I_T\}$
Output: Predicted driver response \mathbf{a}_r and intention \mathbf{a}_i .
 Notice that \mathbf{a}_r consists of confidence scores of *Go* or *Stop*.
 $\mathbf{a}_r := \{r^{go}, r^{stop}\}$.

```

1:  $O := \text{DetectionAndTracking}(I)$ 
    $:= \{O_1, O_2, \dots, O_N\}$  // List of Thing object tracklets
2:  $S := \text{SemanticSegmentation}(I)$ 
    $:= \{S_1, S_2, \dots, S_T\}$  // List of Stuff objects
3: // Data Augmentation via Intervention (Sec. 6.1)
4: if  $\mathbf{A}_r$  is Go and  $N > 1$  then
5:   // Randomly remove a tracklet
    $k := \text{RandomSelect}(N)$ 
6: else
7:    $k$  is empty
8: end if
9: // Mask out Thing object  $k$  on each mask frame
    $M := \text{MaskGenerator}(I, O_k)$ 
10: // Remove a Thing object  $k$  from the tracklet list
    $O' = O - \{O_k\}$ 
11:  $\mathbf{a}_r, \mathbf{a}_i := \text{DrivingModelTraining}(I, M, O', S)$  // Discussed in Sec. 6.1
12: return  $\mathbf{a}_r, \mathbf{a}_i$ 

```

a means for data augmentation to improve the performance of the driving model (Sec. 6.1) and apply causal inference to identify the risk object (Sec. 6.2).

6.1 Driving Model Training with Data Augmentation via Intervention

The performance of driving models depends on the amount of training data under different traffic configurations [26]. Due to limited real-world human driver demonstrations, we propose a novel data augmentation strategy via *intervention* [13]. Specifically, we generate a new data point based on a simple yet effective notion, i.e., removing non-causal objects does not influence driver behavior. For instance, in a *Go* scenario, a driver enters an intersection while pedestrians walk on the sidewalk in an opposite direction. It is reasonable to assume that driver behavior is the same if a pedestrian is not present. Note that, in this work, we only use labeled driver response and intention as the supervision signals. Therefore, the proposed augmentation strategy is only applicable to *Go* scenarios.

In *Stop* scenarios, we need to know causal objects' locations to remove non-causal objects. However, exhaustive risk object labeling is costly, and that is not the focus of this work.

Moreover, even if causal objects are given, we cannot remove causal objects and assume the corresponding driver response to be *Go*, because traffic situations are inherently complicated, so the corresponding driver response is unclear. For instance, a driver is in a congestion situation (i.e., driver stops for the frontal vehicle), and the traffic light of

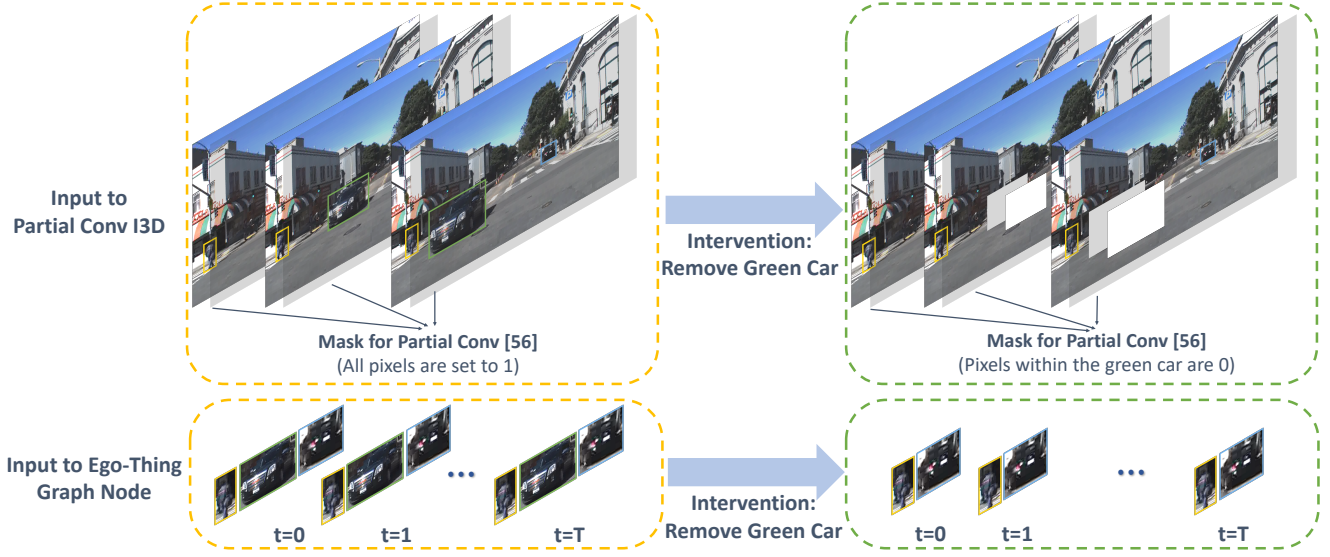


Fig. 6. We simulate a situation using partial convolutional layers [56]. Note that a partial convolutional layer is initially introduced for image inpainting. We utilize partial convolutions to simulate a scenario without the presence of an object. The left-hand side of the figure depicts when an intervention is disabled. To simulate a situation without an object (e.g., the green car in the scene), we set the pixels of the binary mask within the green car's box to 0. In addition, the *Ego-Thing Graph* is constructed without considering the green car as a node.

the driver's lane is red. In this situation, the frontal vehicle is labeled as the risk object (cause). However, driver response remains the same if the frontal vehicle were not present because of the red light. Generating *Stop* scenarios is non-trivial, and we leave it for future works.

To train the intention-aware driving mode with the proposed data augmentation strategy, the model should be able to "intervene," i.e., remove a non-causal object from images. We realize the strategy by replacing standard convolutional layers in I3D with *partial convolutional layers* [56], [57]. Note that a partial convolutional layer is initially introduced for image inpainting. We utilize partial convolutions to simulate a scenario without the presence of an object. A 3D partial convolutional layer takes two inputs, i.e., a sequence of RGB frames and a one-channel binary mask for each frame. The pixel values of a mask are 1 by default. While training the driving model with data augmentation, we set the pixels within the selected object to be 0. In addition, the node of the selected object in a graph is disconnected from the rest of the objects.

The proposed training process is outlined in Algorithm 1. Given training samples in a *Go* scenario, we randomly select an object k to intervene, i.e., simulating a situation without the presence of the object. Specifically, given a tracklet o_k , a one-channel binary mask M_t at time t is defined as

$$M_t(i, j) = \begin{cases} 0, & \text{if } (i, j) \text{ in region } o_k^t, \\ 1, & \text{otherwise} \end{cases}, \quad (7)$$

where o_k^t is the bounding box of the k -th object at time t , and (i, j) is a pixel coordinate within the box. Note that k -th object is discarded from the tracklet list while training the driving model.

Algorithm 2 Causal Inference for Risk Object Identification

T : Number of frames

N : Number of objects

Input: A sequence of RGB frames $I := \{I_1, I_2, \dots, I_T\}$ where the ego car stops

Output: Risk object ID

```

1:  $O := \text{DetectionAndTracking}(I)$ 
    $:= \{O_1, O_2, \dots, O_N\}$  // List of Thing object tracklets
2:  $S := \text{SemanticSegmentation}(I)$ 
    $:= \{S_1, S_2, \dots, S_T\}$  // List of Stuff objects
3: for  $O_k \in O$  do
4:   // Mask out Thing object  $k$  on each frame
    $M := \text{MaskGenerator}(I, O_k)$ 
5:   // Remove the Thing object  $k$  from the tracklet list
    $O' = O - \{O_k\}$ 
6:   // Predict driver response and intention
   without the object  $k$ , where  $\mathbf{a}_r := \{r_k^{go}, r_k^{stop}\}$ 
    $\mathbf{a}_r, \mathbf{a}_i := \text{DrivingModel}(I, M, O', S)$ 
7: end for
8: return  $\arg \max_k (r_k^{go})$ 

```

6.2 Causal Inference for Risk Object Identification

Given a 'Stop' scenario, we aim to identify the corresponding risk object. We deploy the same intervention process discussed in Section 6.1 to identify the risk object. Specifically, the masks of a tracklet and the corresponding video frames are processed by the same driving model. The model outputs the confidence score of *Go* and *Stop* without the presence of the tracklet. After iterating through all tracklets, we select the object with the highest *Go* confidence score to be the risk object. This is because the object causes the most

Model	Response				Intention
	Perplexity	Macro Accuracy	Micro Accuracy	Overall mAP	Overall mAP
1. CNN + LSTM	1.00	64.37	77.95	71.07	/
2. CNN + LSTM + Multi-head	0.93	68.27	79.04	70.12	36.41
3. Pixel-level Attention [7]	0.89	76.15	80.21	78.57	/
4. Object-level Attention [8]	0.84	78.81	83.19	79.02	/
5. GCN (ours)	0.83	77.57	82.64	80.33	/
6. GCN + Multi-head (ours)	0.72	76.30	85.68	<u>84.46</u>	36.31
7. GCN + TRN Head (ours)	<u>0.69</u>	<u>79.32</u>	<u>86.17</u>	<u>83.44</u>	36.80
8. GCN + TRN Head + Data Augmentation (ours)	0.37	87.63	92.56	95.44	<u>36.75</u>

TABLE 2

Results of driver response prediction compared with baselines. Perplexity (lower is better), macro- and micro-average accuracies, and overall mAP are used as metrics for driver response prediction. The unit is % for all metrics except perplexity. The best and second best performances are shown in bold and underlined, respectively. We also report the performance of driver intention prediction using the overall mAP as the metric.

driver behavior change. Algorithm 2 describes the overall causal inference process.

7 EXPERIMENTS

7.1 Implementation Details

We implement our framework in TensorFlow. All experiments are performed on a server with 4 NVIDIA TITAN-XP cards. The input to the framework is a 20-frame clip with a resolution of 224×224 at 3 fps, approximately 6.67s. The framework outputs the predictions of driver intention and response of the very next frame. We adopt Inception-v3 [58] pre-trained on ImageNet [59] as the backbone, following [60] to inflate 2D convolution into a 3D ConvNet, and finetune it on the Kinetics action recognition dataset [61]. The intermediate feature used in RoIAlign and MaskAlign is the *Mixed_3c* layer, where the number of feature channels is 512. The intention feature is generated from a $1 \times 1 \times 1$ convolution on the *Mixed_5c* layer’s feature, and the channel number of the feature is 512. The downsampled binary mask M_t' is 28×28 . The decoder length is set to be 3. The model is trained in a two-stage training scheme with a batch size of 32. First, we finetune the Kinetics pre-trained model on the driver-centric ROI dataset for 50 000 iterations without using GCN. Second, we load the weights trained in the first stage and finetune the network with GCN for another 20 000 iterations. Note that we employ the augmentation strategy mentioned in Section. 6.1 in the second stage. We use the Adam optimizer [62] with the default parameters. The learning rate is set to be 0.001 and 0.0002 for the first and second stage, respectively.

7.2 Driving Model Performance

7.2.1 Evaluation Setup

The performance of the driving model is evaluated as a discrete feasible action prediction, in accordance with [8], [26], [63]. The two discrete actions, *Go* and *Stop* are evaluated. We follow the train/test split defined in [41], [47], where 846 411 and 271 989 samples are used for training and testing, respectively. Four evaluation metrics are utilized. First, we report perplexity as in [8], [26], [63]. Perplexity calculates the negative log-likelihood of predicted probability

of **Response** given ground truth (lower is better). Second, the macro-averaged accuracy is reported. Note that, in a multi-class classification setup, the micro-averaged accuracy is preferable if the label distribution is imbalanced. In our task, the *Go* to *Stop* ratio is approximately 4:1. Therefore, we also report the micro-averaged accuracy as the third metric. **Response** prediction can be treated as an online action detection task [50], [64]. We use per-frame mean average precision (mAP) as the fourth evaluation metric.

7.2.2 Evaluation

Table 2 summarizes the results of the driving models. We compare the following baselines. To compare different models, we keep their backbone network (i.e., Inception-v3) the same.

CNN+LSTM. We extract visual features from the *Mixed_5c* layer of I3D and sequentially input the features at each time step to a two-layer LSTM [50] for temporal modeling.

Pixel-level attention. The pixel-level attention module is proposed by [7] to improve model’s interpretability and the performance of driving models.

Object-level attention. In [8], the authors propose an object-centric attention mechanism to augment end-to-end policy learning. Both pixel- and object-level attention modules are incorporated into **CNN+LSTM**.

The following summarizes our proposals.

GCN. The key difference between GCN and three baselines is the input feature to the LSTM module. Specifically, the feature is processed via Graph Convolution Networks and contains interaction among traffic participants and driver.

Multi-head. We add an additional head for driver intention prediction to **CNN+LSTM** and **GCN**. A standard cross-entropy loss is used for driver intention prediction. Note that both the interaction and intention features share the same features from the *Mixed_5c* layer of I3D.

TRN Head. To forecast future interactions, we incorporate TRN [50]. We initialize TRN with intention representation (as shown in Fig. 5).

Intervention. The concept of intervention is utilized to augment training data to improve the performance of driver response prediction discussed in Section 6.1.

We show that **GCN** outperforms baselines, demonstrating the importance of interaction modeling. By incorporat-

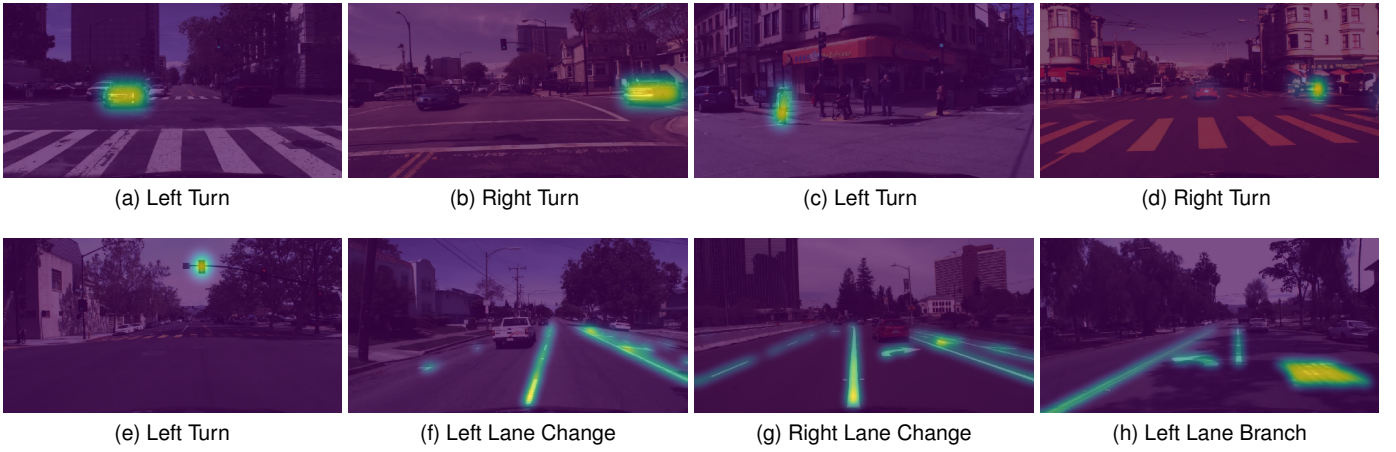


Fig. 7. Visualization of Learned *Ego-Thing Graph* and *Ego-Stuff Graph* on egocentric images. The first and second rows show examples from an *Ego-Thing Graph* and an *Ego-Stuff Graph*, respectively. Comparing (a) and (b), which have similar traffic configurations, our model attends to objects at different locations based on distinct intentions. In (c) and (d), pedestrians intending to cross the street have a significant influence on ego behavior when turning left or turning right. Fig. (e) illustrates a left turn case when the heat map shows high attention around the traffic light, which is green. In (f)-(h), lane markings show strong influences on the ego’s lane-related behaviors.

	Model	Perplexity
Intention Modeling	Without intention modeling	0.83
	Multi-head	0.72
	TRN Head	0.69
Different Graphs	Ego-Stuff Graph	0.74
	Ego-Thing Graph	0.80
	Ego-Thing Graph + Ego-Stuff Graph	0.69
Spatial Modeling	Appearance Relation	0.73
	Appearance + Spatial Relation	0.69
Data Augmentation	Without Augmentation	0.69
	With Augmentation	0.37

TABLE 3
Ablative study of our design choices.

ing **Multi-head**, i.e., intention modeling, both extensions reduce the perplexity by 0.07 and 0.11, respectively. With **TRN Head**, we observe that perplexity is reduced by 0.03. Finally, we demonstrate that **Intervention** significantly improves the performance of the driver response prediction (0.32 decrease in perplexity).

While promising improvements are observed for driver response prediction, the trend does not hold for driver intention prediction, as shown in Table 2. This is because the intention representations used in the four models (Models 1, 6, 7, and 8 listed in Table 2) are features obtained from the *Mixed_5c* layer of I3D, which has negligible gradients in back propagation. A better architectural design for intention prediction is needed, and we leave it for future work.

7.2.3 Ablation Study

We conduct ablation studies to understand the contributions of the proposed architecture designs. The studies are summarized in Table 3.

Analysis of Intention Modeling. The first section of Table 3 analyzes the influence of intention modeling. The baseline does not consider intention. When intention representation

is incorporated into **Multi-head** and **TRN Head**, the results are improved by 0.11 and 0.14, respectively.

Variations of Different Graphs. When both *Ego-Stuff* and *Ego-Thing Graphs* are considered, the model achieves the best perplexity performance. The results indicate the importance of the proposed interaction modeling of drivers, traffic participants, and road infrastructure.

Importance of Spatial Relation. We study the importance of the spatial relation function (Eq. 4) to the **Response** prediction. We conduct two experiments, i.e., 1) using only the appearance relations, and 2) appending 3D spatial relation as an additional constraint. Without using the proposed 3D spatial relation, the perplexity increases by 0.04, indicating the need for a spatial constraint.

Data Augmentation via Intervention. We study the impact of data augmentation by comparing the performance of two models trained with and without the data augmentation strategy. The last section in Table 3 showcases the advantage of using augmented data, cutting the perplexity by nearly half. The data augmentation strategy adds variations to the training set that improve the robustness of the proposed driving model.

7.2.4 Visualization

We visualize learned affinity matrices in *Ego-Thing Graph* and *Ego-Stuff Graph* to determine if our approach can highlight those objects influencing driver behavior. The visualization results as shown in Fig. 7 provide a strong evidence that the proposed model captures the underlying interactions between traffic participants and driver.

Fig. 7a and 7b showcase similar traffic configurations where the driver approaches a four-way intersection with the presence of other vehicles. Given different intentions, i.e., *Left Turn* in Fig. 7a and *Right Turn* in Fig. 7b, our model attends to objects that impact the ego-vehicle navigation. A similar phenomenon is observed in Fig. 7c and 7d. Note that a similar visualization is demonstrated in [47]. Different attention map characteristics are observed. While similar driving model architectures are leveraged, three

Model	$mAcc$			
	Crossing Vehicle	Crossing Pedestrian	Parked Vehicle	Congestion
Random Selection	15.1	7.1	6.4	5.5
Driver's Attention Prediction * [9]	16.8	8.9	10.0	21.3
Object-level Attention * [8]	22.6	9.5	22.6	40.7
Pixel-level Attention * [7]	28.0	8.1	15.6	35.7
GCN (ours)	27.5	13.6	26.0	51.3
GCN + TRN Head (ours)	<u>29.0</u>	<u>13.2</u>	<u>27.3</u>	<u>52.2</u>
GCN + TRN Head + Data Augmentation (ours)	32.5	12.9	28.4	57.5

TABLE 4

Comparison with baselines. The methods with * are re-implemented by us to ensure the same backbone is used for fair comparisons. $mAcc$ stands for mean accuracy, and the unit is %. The best and second best performances are shown in bold and underlined, respectively.

major differences, i.e., different supervision signals, training strategy, and intention-aware design, are introduced in the proposed architectures. Particularly, the additional supervision signal—the driver response, encourages the model attending to object(s) that influence driver behavior.

The bottom row of Fig. 7 represents attention maps obtained from the *Ego-Stuff Graph*. In Fig. 7e, the model captures the relation between driver intention (turning left) and traffic light (green light). Note that we observe that the *Ego-Stuff Graph* modeling captures lane-related driver intention, i.e., *Lane Change*, *Lane Branch* and *Merge*, as shown in Fig. 7f, 7g, and 7h.

7.3 Risk Object Identification

7.3.1 Evaluation Setup

We evaluate risk object identification in the four reactive scenarios: *Congestion*; *Crossing Pedestrian*; *Crossing Vehicle*; and *Parked Vehicle*. We use accuracy (number of correct predictions over the number of samples) as the metric. A correct prediction is one that has an Intersection over Union (IoU) score between a selected box and a ground truth box that is larger than a predefined threshold. Similar to [65], [66], accuracies at IoU thresholds of 0.5 and 0.75 are reported. In addition, mean accuracy ($mACC$) is calculated by using IoU thresholds ranging from 0.5 to 0.95 (in increments of 0.05).

7.3.2 Evaluation

We compare the performance of Risk Object Identification with the following baselines. The results are shown in Table 4.

Random Selection. Random selection randomly picks an object as the risk object from all the detections for a given frame randomly. Note that the method does not process any visual information except object detection. The method is used to contextualize the challenge of this task.

Driver Attention Prediction uses a pre-trained model [9] trained on the BDD-A dataset to predict the driver's gaze attention maps at each frame. We compute an average attention weight of every detected object region based on a predicted attention map. The risk object is the object with the highest attention weight, indicating the driver's gaze attends to this region. The model is trained with human gaze signals that are unavailable in the proposed dataset.

The performance of this method is slightly better than **Random Selection** as reported in the second row of Table 4. We observe that predicted attention maps tend to focus at a vanishing point. Note that this issue has been raised in [10], highlighting the problem as one of the challenges of imitating human gaze behavior.

Object-level Attention Selector. The object-level attention driving model [8] is reformulated for risk object identification. The risk object is the object with the highest object-attention score.

Pixel-level Attention. Kim et al. [7] propose a causality test to search for regions that influence the network's output behavior. Note that region proposals are formed based on sampling predicted pixel-level attention maps. To identify a risk object, we replace the region proposal strategy used in [7] with object detection, and utilize the inferred pixel-level attention map to filter out detections with low attention values. In the experiments, we set the threshold at 0.002. The modification ensures a fair comparison as region proposals obtained from [7] are not guaranteed to be an object entity. Note that the code of region proposal generation detailed in [7] is not publicly available.

We report favorable risk object identification performance over existing baselines [7], [8] in Table 4. The results indicate the effectiveness of the proposed intention-aware driving model and causal inference for the task. In the next section, we perform ablation studies to examine the contributions of each part of our model. Notice that our evaluation protocol differs from [15]. In [15], the authors train four different driving models and test four scenarios independently, whereas a single intention-aware driving model is trained in this work.

7.3.3 Ablation Study

Three variations are studied to analyze their impacts on the performance of risk object identification: (1) architecture of the driving model, (2) intention modeling and (3) training strategy. The results are summarized in Table 5.

Architecture The completed framework (GCN + TRN Head, reported in the last row of Table 5) boosts the $mACC$ s of GCN by 6.2%, 0.5%, 3.0% and 24.6% in four different scenarios, respectively. The architecture ranks first in three scenarios (*Crossing Vehicle*, *Parked Vehicle*, and *Congestion*). We found interaction modeling is crucial, as it improves performance over a pure CNN+LSTM model.

Intention Modeling Both multi-head and TRN head based intention modelings improve overall performance. While the two modelings have similar risk object identification results, we choose TRN Head because it achieves better performance of the driver response prediction task.

Training with Data Augmentation We observe significant improvement in all scenarios with the proposed data augmentation strategy except *Crossing Pedestrian*. The results indicate the effectiveness of the proposed training strategy. For *Crossing Pedestrian*, our conjecture is that vehicles are likely to be chosen because of the natural imbalanced distribution in the training data. Note that the ratio of detected vehicles to pedestrians is approximately 17:1. Our model learns how to identify risk objects under traffic configurations (especially different vehicle configurations) so that the model performs favorably for scenarios that involve

Driving Model	Data Augmentation	Causal Inference	Crossing Vehicle			Crossing Pedestrian			Parked Vehicle			Congestion		
			$Acc_{0.5}$	$Acc_{0.75}$	$mAcc$	$Acc_{0.5}$	$Acc_{0.75}$	$mAcc$	$Acc_{0.5}$	$Acc_{0.75}$	$mAcc$	$Acc_{0.5}$	$Acc_{0.75}$	$mAcc$
CNN + LSTM	✗	✓	29.9	29.9	26.3	15.5	14.3	12.4	33.1	28.7	25.4	39.4	35.4	32.9
GCN (ours)	✗	✓	31.8	31.5	27.5	<u>16.7</u>	15.5	<u>13.6</u>	32.4	29.4	26.0	56.6	56.6	51.3
GCN + Multi-head (ours)	✗	✓	31.8	31.8	28.0	17.9	17.9	14.6	32.4	29.4	26.3	61.6	57.6	53.8
GCN + TRN Head (ours)	✗	✓	<u>33.1</u>	<u>33.1</u>	<u>29.0</u>	<u>16.7</u>	<u>16.7</u>	13.2	<u>33.8</u>	<u>30.2</u>	<u>27.3</u>	60.6	56.6	52.2
GCN + TRN Head (ours)	✓	✗	28.3	28.0	25.0	13.1	11.9	9.6	22.1	21.3	18.7	<u>65.7</u>	<u>61.6</u>	<u>57.4</u>
GCN + TRN Head (ours)	✓	✓	37.0	37.0	32.5	15.5	15.5	12.9	35.3	31.6	28.4	66.7	62.6	57.5

TABLE 5

Ablation study of the proposed risk object identification framework. The unit is %. The best and second best performances are shown in bold and underlined, respectively.

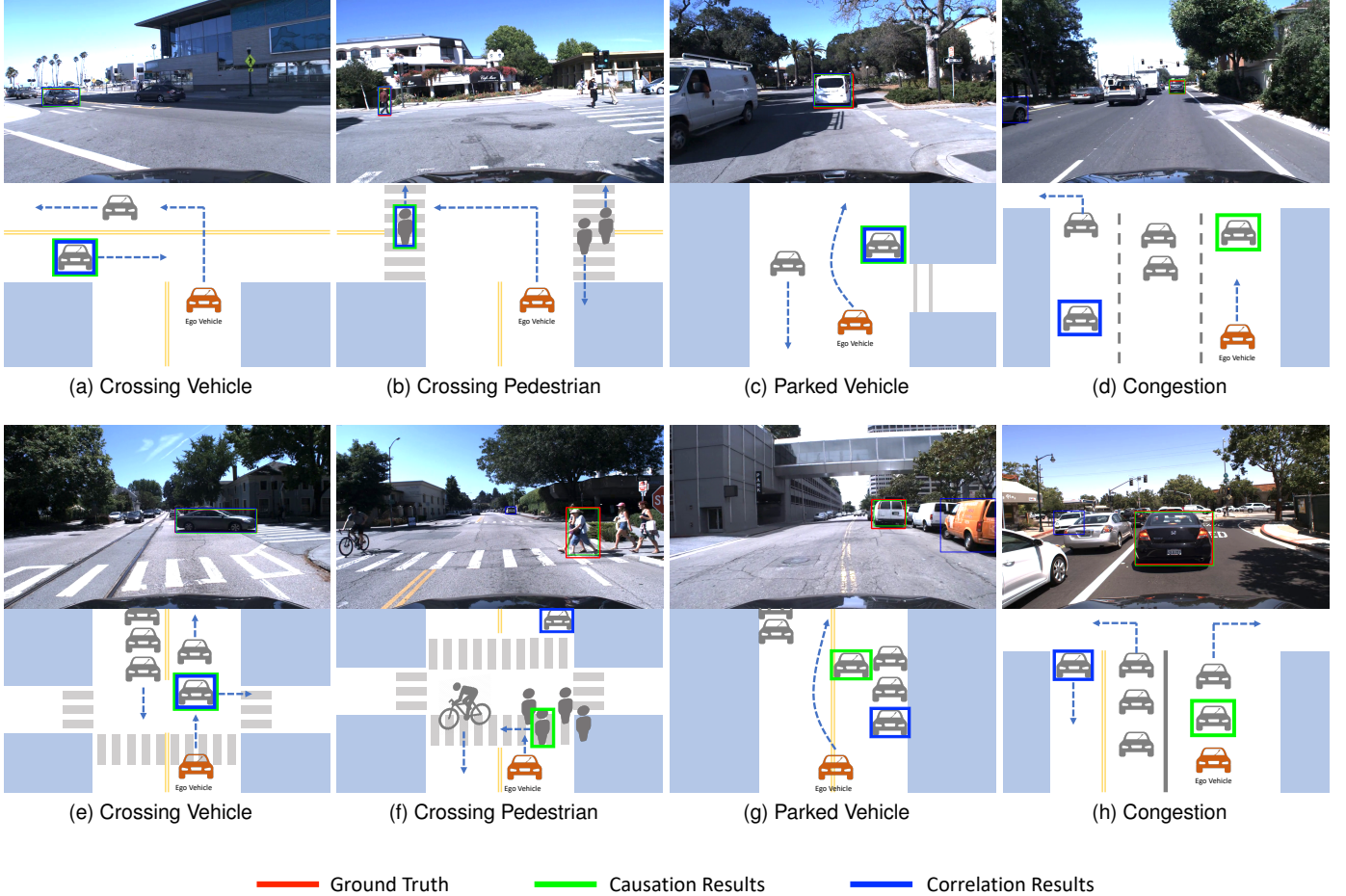


Fig. 8. Risk object identification results obtained by **Causation** and **Correlation**. Note that **Causation** is the causal inference based approach proposed in the paper. Instead of using causal inference, **Correlation** determines the risk object by selecting the object with the highest attention weight to *Ego* in the *Ego-Thing Graph*. The top row shows an egocentric view where green boxes indicate our **Causation** results, blue boxes are **Correlation** results, and ground truth boxes are in red. A bird's-eye-view representation is presented in the bottom row, providing information including scene layout and intentions of traffic participants.

interacting with vehicles. In contrast, scenarios that involve interacting with pedestrians are less emphasized. To solve this problem, a possible solution is to perform a category-aware intervention so that a balanced distribution can be obtained.

In summary, with the proposed components, i.e., TRN Head, intention modeling, and training with data augmentation, we demonstrate state-of-the-art risk object identification performance. Note that this observation is also found

in driver response prediction, discussed in Section 7.2.

7.3.4 Correlation vs. Causation

We study the importance of causal modeling for this task. Instead of using causal inference (called **Causation**) to identify the risk object, the risk object is the object with the highest attention weight between *Ego* in *Ego-Thing Graph*. We call this method **Correlation**. In Table 5, the second to the last row shows the results of **Correlation**. Our **Causation** ap-

proach significantly outperforms **Correlation** in all reactive scenarios. We empirically demonstrate the need of casual modeling for this task.

In Fig. 8, ground truth risk objects are enclosed in red bounding boxes, our **Causation** results are shown in green, and the **Correlation** predictions are shown in blue boxes. In addition, we provide a bird's-eye-view (BEV) pictorial illustration of scenes in the second row. Note that BEVs depict scene layouts, driver intention, and traffic participants' intentions, with identified risk objects in green boxes. In Fig. 8 (b), three crossing pedestrians with different intentions are depicted. Our **Causation** approach correctly identifies the left-hand side pedestrian as the risk object while the driver intends to turn left. While **Correlation** predicts the same result, our method is more explainable because the decision is made by considering driver intention. Fig. 8 (d), (f), (g) and (h) showcase examples where **Correlation** fails but the proposed framework identifies risk objects successfully.

8 CONCLUSION

In this paper, we propose a novel driver-centric definition of risk, i.e., risky objects influence driver behavior. A new task called risk object identification is introduced and is formulated as a cause-effect problem. We present a novel two-stage risk object identification framework inspired by the model of situation awareness and causal inference. We also create a driver-centric Risk Object Identification (ROI) dataset to evaluate the proposed system. Extensive quantitative and qualitative evaluations are conducted. Favorable performance compared with strong baselines is demonstrated. Future work can leverage road topology explicitly to improve driver intention prediction. Additionally, a single shot risk object identification framework would be interesting to explore for practical applications.

ACKNOWLEDGMENTS

The work is sponsored by Honda Research Institute USA.

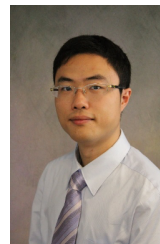
REFERENCES

- [1] World Health Organization, "Global status report on road safety 2018: Summary," 2018.
- [2] "NHTSA," <https://www.nhtsa.gov/research/>.
- [3] S. Lefèvre, D. Vasquez, and C. Laugier, "A Survey on Motion Prediction and Risk Assessment for Intelligent Vehicles," *ROBOMECH Journal*, vol. 1, p. 1, 2014.
- [4] S. Alletto, A. Palazzi, F. Solera, S. Calderara, and R. Cucchiara, "DR(eye)VE: A Dataset for Attention-based Tasks with Applications to Autonomous and Assisted Driving," in *IEEE Conference on Computer Vision and Pattern Recognition Workshop*, 2016.
- [5] M. Gao, A. Tawari, and S. Martin, "Goal-oriented Object Importance Estimation in On-road Driving Videos," in *IEEE International Conference on Robotics and Automation*, 2019.
- [6] K.-H. Zeng, S.-H. Chou, F.-H. Chan, J. C. Niebles, and M. Sun, "Agent-Centric Risk Assessment: Accident Anticipation and Risky Region Localization," in *IEEE Conference on Computer Vision and Pattern Recognition*, 2017.
- [7] J. Kim and J. Canny, "Interpretable Learning for Self-driving Cars by Visualizing Causal Attention," in *IEEE International Conference on Computer Vision*, 2017.
- [8] D. Wang, C. Devin, Q.-Z. Cai, F. Yu, and T. Darrell, "Deep Object Centric Policies for Autonomous Driving," in *IEEE International Conference on Robotics and Automation*, 2019.
- [9] Y. Xia, D. Zhang, J. Kim, and D. W. Ken Nakayama, Karl Zipser, "Predicting Driver Attention in Critical Situations," in *Asian Conference on Computer Vision*, 2018.
- [10] A. Tawari, P. Mallela, and S. Martin, "Learning to Attend to Salient Targets in Driving Videos using Fully Convolutional RNN," in *IEEE Intelligent Transportation Systems Conference*, 2018.
- [11] B. Tatler, M. Hayhoe, M. Land, and D. Bal-lard, "Eye Guidance in Natural Vision: Reinterpreting Saliency," *Journal of Vision*, vol. 11, p. 5, 2011.
- [12] P. de Haan, D. Jayaraman, and S. Levine, "Causal Confusion in Imitation Learning," in *IEEE Conference on Neural Information Processing Systems*, 2019.
- [13] J. Pearl, "Causality," *Cambridge University Press*, 2009.
- [14] M. R. Endsley, "Theoretical Underpinnings of Situation Awareness: A Critical Review," in *Situation Awareness Analysis*, 2000.
- [15] C. Li, S. H. Chan, and Y.-T. Chen, "Who Make Drivers Stop? Towards Driver-centric Risk Assessment: Risk Object Identification via Causal Inference," *IEEE International Conference on Robotics and Automation*, 2020.
- [16] J. Ibanez-Guzman, S. Lefevre, A. Mokkadem, and S. Rodhaim, "Vehicle to vehicle communications applied to road intersection safety, field results," in *13th International IEEE Conference on Intelligent Transportation Systems*. IEEE, 2010, pp. 192–197.
- [17] S. Worrall, D. Orchansky, F. Masson, and E. Nebot, "Improving Vehicle Safety using Context based Detection of Risk," in *IEEE International Conference on Intelligent Transportation Systems*. IEEE, 2010, pp. 379–385.
- [18] A. Chinae and M. Parent, "Risk assessment algorithms based on recursive neural networks," in *2007 International Joint Conference on Neural Networks*. IEEE, 2007, pp. 1434–1440.
- [19] F. D. Salim, S. W. Loke, A. Rakotonirainy, B. Srinivasan, and S. Krishnaswamy, "Collision pattern modeling and real-time collision detection at road intersections," in *2007 IEEE Intelligent Transportation Systems Conference*. IEEE, 2007, pp. 161–166.
- [20] M. Althoff and A. Mergel, "Comparison of Markov chain abstraction and Monte Carlo simulation for the safety assessment of autonomous cars," *IEEE Transactions on Intelligent Transportation Systems*, vol. 12, no. 4, pp. 1237–1247, 2011.
- [21] D. Greene, J. Liu, J. Reich, Y. Hirokawa, A. Shinagawa, H. Ito, and T. Mikami, "An efficient computational architecture for a collision early-warning system for vehicles, pedestrians, and bicyclists," *IEEE Transactions on intelligent transportation systems*, vol. 12, no. 4, pp. 942–953, 2011.
- [22] A. Lawitzky, D. Althoff, C. F. Passenberg, G. Tanzmeister, D. Wollherr, and M. Buss, "Interactive scene prediction for automotive applications," in *2013 IEEE Intelligent Vehicles Symposium (IV)*. IEEE, 2013, pp. 1028–1033.
- [23] S. Lefèvre, C. Laugier, and J. Ibañez-Guzmán, "Evaluating Risk at Road Intersections by Detecting Conflicting Intentions," in *International Conference on Intelligent Robots and Systems*, 2012.
- [24] D. A. Pomerleau, "AIVINN: An Autonomous Land Vehicle in a Neural Network," in *Technical report, Carnegie Mellon University, Computer Science Department*, 1989.
- [25] M. Bojarski, D. D. Testa, D. Dworakowski, B. Firner, B. Flepp, P. Goyal, L. D. Jackel, M. Monfort, U. Muller, J. Zhang, X. Zhang, J. Zhao, and K. Zieba, "End to End Learning for Self-Driving Cars," in *arXiv preprint arXiv:1604.07316*, 2016.
- [26] H. Xu, Y. Gao, F. Yu, and T. Darrell, "End-To-End Learning of Driving Models From Large-Scale Video Datasets," in *IEEE Conference on Computer Vision and Pattern Recognition*, 2016.
- [27] J. Kim, T. Misu, Y.-T. Chen, A. Tawari, and J. Canny, "Grounding Human-to-vehicle Advice for Self-driving Vehicles," in *IEEE Conference on Computer Vision and Pattern Recognition*, 2019.
- [28] A. Alahi, V. Ramanathan, and L. Fei-Fei, "Socially-aware Large-scale Crowd Forecasting," in *IEEE Conference on Computer Vision and Pattern Recognition*, 2014.
- [29] A. Alahi, K. Goel, V. Ramanathan, A. Robicquet, L. Fei-Fei, and S. Savarese, "Social LSTM: Human Trajectory Prediction in Crowded Spaces," in *IEEE Conference on Computer Vision and Pattern Recognition*, 2016.
- [30] A. Gupta, J. Johnson, L. Fei-Fei, S. Savarese, and A. Alahi, "Social GAN: Socially Acceptable Trajectories with Generative Adversarial Networks," in *IEEE Conference on Computer Vision and Pattern Recognition*, 2018.
- [31] Y. Xu, Z. Piao, and S. Gao, "Encoding Crowd Interaction with Deep Neural Network for Pedestrian Trajectory Prediction," in *IEEE Conference on Computer Vision and Pattern Recognition*, 2018.

- [32] F. Codevilla, M. Miiller, A. López, V. Koltun, and A. Dosovitskiy, "End-to-end Driving via Conditional Imitation Learning," in *IEEE International Conference on Robotics and Automation*, 2018.
- [33] F. Codevilla, E. Santana, A. M. López, and A. Gaidon, "Exploring the limitations of behavior cloning for autonomous driving," 2019.
- [34] J. Pearl, M. Glymour, and N. P. Jewell, *Causal inference in statistics: A primer*. John Wiley & Sons, 2016.
- [35] S. Nair, Y. Zhu, S. Savarese, and L. Fei-Fei, "Causal Induction from Visual Observations for Goal Directed Tasks," in *NeurIPS 2019 Workshop on Causal Machine Learning*, 2019.
- [36] Y. Li, A. Torralba, D. F. Animashree Anandkumar, and A. Garg, "Causal Discovery in Physical Systems from Videos," in *Conference on Neural Information Processing Systems*, 2020.
- [37] J. Qi, Y. Niu, J. Huang, and H. Zhang, "Two Causal Principles for Improving Visual Dialog," in *IEEE Conference on Computer Vision and Pattern Recognition*, 2020.
- [38] T. Wang, J. Huang, H. Zhang, and Q. Sun, "Visual Commonsense R-CNN," in *IEEE Conference on Computer Vision and Pattern Recognition*, 2020.
- [39] X. Yang, H. Zhang, and J. Cai, "Deconfounded Image Captioning: A Causal Retrospect," in *arXiv preprint arXiv:2003.03923*, 2020.
- [40] J. Hawke, R. Shen, C. Gurau, S. Sharma, D. Reda, N. Nikolov, P. Mazur, S. Micklethwaite, N. Griffiths, A. Shah, and A. Kendall, "Urban Driving with Conditional Imitation Learning," in *arXiv preprint arXiv:1912.00177*, 2019.
- [41] V. Ramanishka, Y.-T. Chen, T. Misu, and K. Saenko, "Toward Driving Scene Understanding: A Dataset for Learning Driver Behavior and Causal Reasoning," in *IEEE Conference on Computer Vision and Pattern Recognition*, 2018.
- [42] K. He, G. Gkioxari, P. Dollar, and R. Girshick, "Mask R-CNN," in *IEEE Conference on Computer Vision and Pattern Recognition*, 2017.
- [43] S. Rota Bulò, L. Porzi, and P. Kotschieder, "In-place activated batchnorm for memory-optimized training of dnns," in *Proceedings of the IEEE Conference on Computer Vision and Pattern Recognition*, 2018.
- [44] N. Wojke, A. Bewley, and D. Paulus, "Simple Online and Realtime Tracking with a Deep Association Metric," in *2017 IEEE International Conference on Image Processing*, 2017.
- [45] R. Ranftl, K. Lasinger, D. Hafner, K. Schindler, and V. Koltun, "Towards robust monocular depth estimation: Mixing datasets for zero-shot cross-dataset transfer," *IEEE Transactions on Pattern Analysis and Machine Intelligence (TPAMI)*, 2020.
- [46] T. N. Kipf and M. Welling, "Semi-supervised Classification with Graph Convolutional Networks," in *IEEE International Conference on Learning Representations*, 2017.
- [47] C. Li, Y. Meng, S. H. Chan, and Y.-T. Chen, "Learning 3D-aware Egocentric Spatial-Temporal Interaction via Graph Convolutional Networks," in *IEEE International Conference on Robotics and Automation*, 2020.
- [48] J. Wu, L. Wang, L. Wang, J. Guo, and G. Wu, "Learning Actor Relation Graphs for Group Activity Recognition," in *IEEE Conference on Computer Vision and Pattern Recognition*, 2019.
- [49] J. L. Ba, J. R. Kiros, and G. E. Hinton, "Layer Normalization," in *arXiv preprint arXiv:1607.06450*, 2016.
- [50] M. Xu, M. Gao, Y.-T. Chen, L. Davis, and D. Crandall, "Temporal Recurrent Networks for Online Action Detection," in *IEEE International Conference on Computer Vision*, 2019.
- [51] S. Hochreiter and J. Schmidhuber, "Long Short-term Memory," *Neural computation*, 1997.
- [52] X. Wang and A. Gupta, "Videos as Space-Time Region Graphs," in *IEEE European Conference on Computer Vision*, 2018.
- [53] S. Yan, Y. Xiong, and D. Lin, "Spatial Temporal Graph Convolutional Networks for Skeleton-Based Action Recognition," in *AAAI Conference on Artificial Intelligence*, 2018.
- [54] A. Rahimpour, S. Martin, A. Tawari, and H. Qi, "Context Aware Road-user Importance Estimation (iCARE)," in *IEEE Intelligent Vehicles Symposium*, 2019.
- [55] S. Lefèvre, C. Laugier, and J. Ibañez-Guzmán, "Intention-aware Risk Estimation for General Traffic Situations, and Application to Intersection Safety," 2013.
- [56] G. Liu, a. K. J. S. Fitsum A. Reda, T.-C. Wang, A. Tao, and B. Catanzaro, "Image Inpainting for Irregular Holes using Partial Convolutions," in *IEEE European Conference on Computer Vision*, 2018.
- [57] G. Liu, K. J. Shih, T.-C. Wang, F. A. Reda, K. Sapra, Z. Yu, A. Tao, and B. Catanzaro, "Partial Convolution based Padding," *arXiv preprint arXiv:1811.11718*, 2018.
- [58] C. Szegedy, V. Vanhoucke, S. Ioffe, J. Shlens, and Z. Wojna, "Rethinking the Inception Architecture for Computer Vision," in *IEEE Conference on Computer Vision and Pattern Recognition*, 2016.
- [59] O. Russakovsky, J. Deng, H. Su, J. Krause, S. Satheesh, S. Ma, Z. Huang, A. Karpathy, A. Khosla, M. Bernstein, A. C. Berg, and L. Fei-Fei, "ImageNet LargeScale Visual Recognition Challenge," in *International Journal of Computer Vision*, 2015.
- [60] J. Carreira and A. Zisserman, "Quo Vadis, Action Recognition? A New Model and the Kinetics Dataset," in *IEEE Conference on Computer Vision and Pattern Recognition*, 2017.
- [61] W. Kay, J. Carreira, K. Simonyan, B. Zhang, C. Hillier, S. Vijayanarasimhan, F. Viola, T. Green, T. Back, P. Natsev, M. Suleyman, and A. Zisserman, "The Kinetics Human Action Video Dataset," in *arXiv preprint arXiv:1705.06950*, 2017.
- [62] D. P. Kingma and J. Ba, "Adam: A Method for Stochastic Optimization," in *arXiv preprint arXiv:1412.6980*, 2014.
- [63] D. Wang, C. Devin, Q.-Z. Cai, P. Krähenbühl, and T. Darrell, "Monocular Plan View Networks for Autonomous Driving," in *International Conference on Intelligent Robots and Systems*, 2019.
- [64] R. De Geest, E. Gavves, A. Ghodrati, Z. Li, C. Snoek, and T. Tuytelaars, "Online Action Detection," in *IEEE European Conference on Computer Vision*, 2016.
- [65] T.-Y. Lin, M. Maire, S. Belongie, J. Hays, P. Perona, D. Ramanan, P. Dollár, and C. L. Zitnick, "Microsoft COCO: Common Objects in Context," in *IEEE European Conference on Computer Vision*, 2014.
- [66] Z. Zhang, C. Yu, and D. Crandall, "A Self Validation Network for Object-Level Human Attention Estimation," in *IEEE Conference on Neural Information Processing Systems*, 2019.



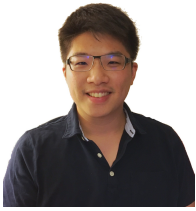
Chengxi Li received her B.S. degree (2016) in Electrical Engineering from Fudan University in Shanghai, China. She is currently a Ph.D. student in the School of Electrical and Computer Engineering at Purdue University, IN, USA. Her research interests lie at the intersection of machine learning and computer vision.



Stanley H. Chan (S'06–M'12–SM'17) received a B.Eng. degree (with first class honors) in Electrical Engineering from the University of Hong Kong in 2007, a M.A. degree in Mathematics from the University of California at San Diego in 2009, and a Ph.D. degree in Electrical Engineering from the University of California at San Diego in 2011. From 2012 to 2014, he was a postdoctoral research fellow at Harvard John A. Paulson School of Engineering and Applied Sciences. He is currently an associate professor in the School

of Electrical and Computer Engineering and the Department of Statistics at Purdue University, West Lafayette, IN.

Dr. Chan is a recipient of the Best Paper Award of IEEE International Conference on Image Processing 2016, IEEE Signal Processing Cup 2016 Second Prize, Purdue College of Engineering Exceptional Early Career Teaching Award 2019, Purdue College of Engineering Outstanding Graduate Mentor Award 2016, and Eta Kappa Nu (Beta Chapter) Outstanding Teaching Award 2015. He is also a recipient of the Croucher Foundation Fellowship for Postdoctoral Research 2012–2013 and the Croucher Foundation Scholarship for Ph.D. Studies 2008–2010. His research interests include computational imaging and machine learning.



Yi-Ting Chen received a B.S. degree in Electronics Engineering from National Chiao Tung University, Hsinchu, Taiwan and a Ph.D. degree from the Department of Electrical and Computer Engineering at Purdue University in 2015. He was a senior scientist at Honda Research Institute USA from 2015 to 2020. He is currently an assistant professor in the Department of Computer Science at National Yang Ming Chiao Tung University, Hsinchu, Taiwan. His research interests lie in computer vision, machine learning, robotics, and behavior science, and their applications to intelligent driving systems and assistive robotics.